Journal of Engineering Physics and Thermophysics, Vol. 77, No. 1, 2004

A CONTRIBUTION TO THE THEORY OF POROSITY OF FINE-GRAINED SEDIMENTS

J. G. Dueck,[a] D. Purevjav,[b] and D. Yu. Kilimnik[c]

UDC 539.6,539.217

The influence of adhesive forces on the structure of sedimentation layers has been considered. A theoretical model allowing calculation of the porosity of a sedimentation layer as a function of the particle size, the layer thickness, and the adhesive-force level has been developed. Experiments in which these variables were changed have been carried out. The adhesive force was varied by changing the concentration of the electrolyte. A quantitative agreement between theory and experiment is observed for the porosity as a function of the particle size and the layer thickness; for the porosity as a function of the adhesive force this agreement is qualitative.

Sediments, i.e., layers of a settled dispersed material, occur in nature (for example, the bottom and banks of a water reservoir) [1] and in technology (settlers and filtered beds) [2]. The density of sediments and accordingly their porosity are an important characteristic for evaluations of their mobility or moisture content. It is common knowledge that the porosity of one and the same material depends on the ionic strength and ζ potential of the particle surface, which can be changed by variation of the parameters of the liquid phase [3, 4]. Such a dependence is caused by adhesive forces. Common understanding of this circumstance was reached long ago, but there is still no quantitative description of the effects which allows computation of the structural characteristics of a dispersed-material layer.

We know of successful attempts at describing semiquantitatively the structure of a sediment on the basis of fractal notions but without using specific expressions for forces acting between particles [5]. A theoretical description of the sediment structure has been approached very closely by Taki [6], who used the Derjagin–Landau–Verwey–Overbeek (DLVO) equations for the potential of adhesive forces in computation of a critical gradient of the water velocity at the boundary between the flow and the layer, which is sufficient for erosion of the sediment. But he, too, did not seek to compute the porosity of the sediment.

In [7, 8], the porosity has been computed on the basis of the DLVO theory as applied to the problem of filtration. Theoretical calculations presented in [7, 8] are based on the balance of forces acting on the particles in a filtered bed. When a motionless sediment is considered, hydrodynamic forces drop out of analysis. Otherwise the theory developed in [7, 8] must describe the influence of adhesive forces on the sediment structure.

The discussion given below is devoted to a theoretical and experimental study of the influence of the interparticle interaction in the layer on the porosity of sediments.

Interaction of Particles in a Sediment Layer. The interaction between two identical spherical particles in an aqueous solution can be described within the DLVO theory [9–11] by the combined force potential

$$W = W_{\text{at}} + W_{\text{r}} ,$$

composed of the van der Waals attractive potential

$$W_{\text{at}} = -\frac{A}{12h} d_{\text{p}}$$

[a]Erlangen-Nürnberg University (Universität Erlangen-Nürnberg), D-91052, Erlangen, Germany; email: Johan.Dueck@uvt.cbi.uni_erlangen.de; [b]Mongolian State University of Science and Technology, Ulan Bator-46, Mongolia; [c]N. É. Bauman Moscow State Technical University, 5 2nd Baumanskaya Str., Moscow, 107005, Russia. Translated from Inzhenerno-Fizicheskii Zhurnal, Vol. 77, No. 1, pp. 77–85, January–February, 2004. Original article submitted August 6, 2003.

1062-0125/04/7701-0093 ©2004 Plenum Publishing Corporation

and the repulsive potential according to the Gouy–Chapman theory (for the sake of simplicity it has been assumed that there are ions just of one sort)

$$W_r = \frac{32\pi kTd_p c_\infty}{\kappa^2}\gamma^2 \exp[-\kappa h] .$$

Next we introduce the Debye length

$$\frac{1}{\kappa} = \sqrt{\frac{\varepsilon\varepsilon_0 kT}{e^2 c_\infty z^2}} ,$$

and finally we have

$$\gamma = \tanh\left[z\frac{e\psi_0}{4kT}\right].$$

Depending on the value of ψ_0, we can single out two limiting cases: $\gamma = e\psi_0/(4kT)$ when $\psi_0 << kT/e$ (practically when $\psi_0 \le 25$ mV, see [9]) and $\gamma = 1$ for $\psi_0 >> kT/e$ when $\psi_0 >> kT$ (i.e., for $\psi_0 \ge 100$ mV).

An analysis of the potential W as a function of h can be found in [9, 10, 12, 13]. For our purposes, it is better to pass to consideration of the interaction forces directly.

The adhesive force $F_{ad} = \partial W/\partial h$ is made up of two components: $F_{ad} = F_{at} + F_r$. In this sum, F_{at} represents the attracting component of one particle to another, $F_{at} = \frac{\Delta}{12h^2} d_p$, and for the repelling force F_r we can write

$$F_r = -\frac{2\pi z^2 e^2}{kT}\psi_0^2 \frac{c_\infty}{\kappa}\exp[-\kappa h]\, d_p . \qquad (1)$$

It is remarkable that the forces F_{at} and F_r are in proportion to the particle diameter. Therefore, the ratio of the total adhesive force F_{ad} to the particle diameter d_p can be interpreted as the specific adhesion energy $E = F_{ad}/d_p$ characterizing the physicochemical state of a suspension and determining the properties of a sediment [10].

The surface potential ψ_0 on quartz particles in water is negative and can approximately be evaluated through measurements of the ζ potential [9, 11].

Direct employment of the equations of the DLVO theory is bounded by the uncertainty of the quantity h. It cannot be found within the theory itself. One usually assumes that the distance h is equal to the size of an H_2O molecule and is taken to be 0.4 nm [10, 13]. This quantity can be justified by the existence of forces not considered by the DLVO theory, in particular, by the repelling forces of Born, which are characterized by a very small radius of action [9]. Unfortunately, there are no general equations allowing computation of the Born force. In any case, this force is independent of the particle size. For example, the power law for it [9], $F_B = -n\frac{d_m^n}{h^{n+1}}$, $6 < n < 12$, contains only the size of a molecule d_m involved in repulsion. The Born, force may not be considered for distances $h > d_m$, and the relation of the forces F_{at} and F_r determines the tendency to coagulation.

The condition of equality of the forces F_{at} and F_r and their potentials [9], leads to the Schulz–Hardy rule for the critical concentration of coagulation c_{cr} that states that c_{cr} is in inverse proportion to the sixth power of the value of the valence z of counterions in the electrolyte:

$$c_{cr} \propto z^{-6} . \qquad (2)$$

It is of interest to note that the critical conditions of coagulation in the sense indicated occur when the distance between the particles is equal to the Debye length $1/\kappa$ and this is one to two orders of magnitude larger than the H_2O-

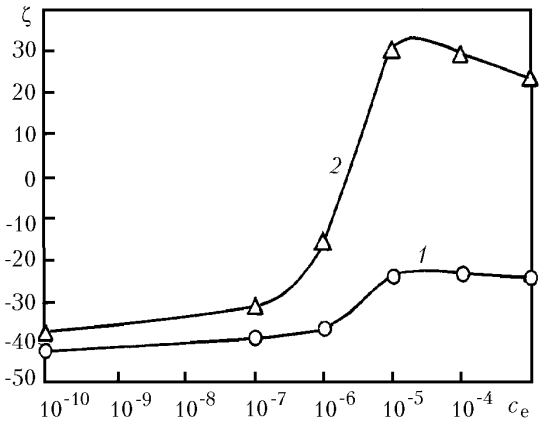

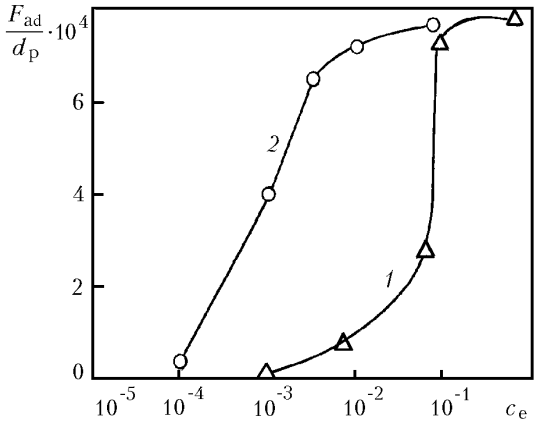

Fig. 1. Change in the ζ potential on the quartz-sand surface as a function of the concentration of the electrolyte: 1) $NaCl_2$; 2) $AlCl_3$.

Fig. 2. Change in the energy of adhesion between glass particles as a function of the concentration of the electrolyte: 1) NaCl; 2) $MgCl_2$.

molecule size. This is another argument in favor of the fact that in consideration of adhesion, one should evaluate *h* beyond the DLVO theory.

The attractive force is not related to the number of cations in the solution, whereas the repulsive force, in accordance with (1), is in proportion to $\psi_0^2 z\sqrt{c_\infty}\ \exp(-\beta z\sqrt{c_\infty})$, β = const, and hence depends on the properties of the electrolyte. Even if the surface potential ψ_0 remains constant, the repulsive force decreases because of the exponential dependence if the concentration of the electrolyte grows. The quantity ψ_0^2 usually drops with increase in the electrolyte concentration because of the adsorption of counterions on the surface.

Figure 1 gives the results of measurements of the ζ potential for fine-grained quartz sand (method of electrophoresis with the use of a ZetaSizer device (Malvern Corp.)). Bivalent magnesium chloride and trivalent aluminum chloride were taken as the electrolyte. In the latter case, there is an isoelectric point at $c_e \approx 5\cdot10^{-5}$ mole/liter upon attainment of which the surface is recharged and the potential changes its sign. For the repulsive force the sign of the potential is of no importance; of importance is the square of this quantity, which drops with growth in the electrolyte concentration except for the interval in the vicinity of the isoelectric point. Therefore, it should be expected that the adhesive force F_{ad} will increase with the concentration of cations, which leads to a growth in the agglomerate size and to a growth in porosity, as will be shown.

Direct measurements of the adhesive force by the method of atomic-force microscopy (AFM), where the forces of interaction between two particles are determined from the deformation of a calibrated piezoelectric element, are fairly difficult [9, 10, 14, 15], which is primarily due to the high requirements of resolution of measurements (of the order of 10^{-8} N relative to the force and of the order of nm relative to displacements). Certain difficulties also arise in interpretation of measurements. Measurements by the centrifugal method [13] are less precise but simpler. One measures the threshold of rotational velocity of a centrifuge for which there begins mass-scale separation of particles previously applied to the rotating-substrate surface facing the exterior wall of the apparatus. It is precisely the results of measurements by this method that will be used in what follows, since they contain data for SiO_2–H_2O–SiO_2-based materials similar to those employed below. The vibration method [12] somewhat combines the centrifugal method (criterion: separation of a particle from the substrate under the action of the vibration force) and the AFM method (monitoring of particle motion with a microscope with digital recording of measurements). The results of the experiments [12, 13] in principle confirm the dependence of the adhesive force on the particle size for different combinations of aqueous solutions and the materials of particles (glass [12, 13], tin, and aerosil [12]) and the substrate (glass [13] and silicone [12]).

Figure 2 gives experimental dependences of the adhesive energy on the concentration of uni- and bivalent electrolytes [12]. In these and in other similar cases there is a threshold concentration for which this force grows abruptly. One usually relates the threshold concentration to the minimum of the repelling force (or to its total disappearance), which is also due to the attainment of the minimum of the square of the surface potential (or the isoelectric

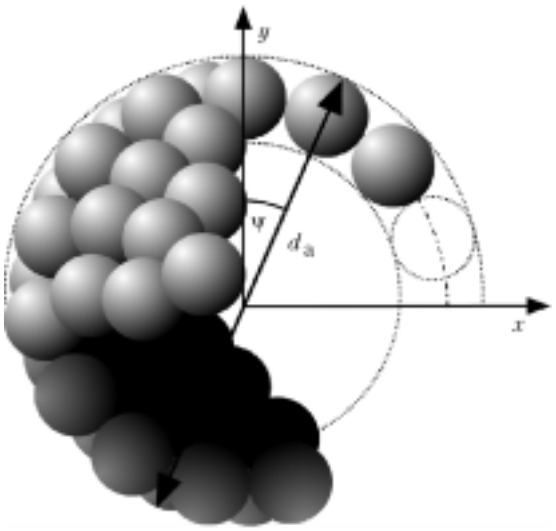

Fig. 3. Structural scheme of the agglomerate.

point). A comparison of Figs. 1 and 2 points to a certain correlation between the values of the ζ potential and the adhesion energy, but an abrupt change in F_{ad} occurs for substantially higher values of the concentration of the electrolyte than those for the minimum of the ζ potential. Therefore, although knowledge of the values of the ζ potential is very useful for a qualitative analysis of the experiments, one should resort, where possible, to comparisons to direct measurements of adhesive forces.

Model of a Compressible Sediment Layer. The interparticle interactions of small suspended particles are determined by both the properties of the solid-phase surface and the concentration and charge of ions in the liquid phase. This interaction causes agglomeration determining the sediment structure. To predict the size of an agglomerate we assume its simplest shape in the form of a hollow sphere of diameter d_a whose shell is formed of the initial particles of size d_p (Fig. 3). Next we assume that all the agglomerates are of the same size and that they form a random packing. This means that the porosity of such a structure takes a value equal to $\varphi_0 = 0.4$.

Let us break the entire volume of the layer into elements (cells) in each of which there is one agglomerate. Thus, each cell is composed of the volume of the agglomerate itself V_a and the remaining volume $V - V_a$. Since the agglomerates form a random packing between themselves, the equation $V = V_a(1 - \varphi_0)$ holds true. Determination of the porosity yields $\varphi = (V - V_p)/V = 1 - (1 - \varphi_0)V_p/V_a$. If n is the number of particles in the agglomerate, we can represent V_p as $V_p = n\pi d_p^3/6$ and express the porosity as

$$\varphi = 1 - n\,(1 - \varphi_0)\,\frac{\pi d_p^3}{6V_a} = 1 - n\,(1 - \varphi_0)\left(\frac{d_p}{d_a}\right)^3 . \tag{3}$$

We can also determine n additionally from the volume of the shell of the postulated agglomerate $V_p = ad_a^2 d_p$, so that $ad_a^2 d_p = nd_p^3$. Therefore, we have $n = a(d_a/d_p)^2$. Here a is the parameter dependent on the density of the packing in the agglomerate's shell. Substitution of n into Eq. (3) yields $\varphi = 1 - a(1 - \varphi_0)(d_p/d_a)$. The parameter a can be determined from the condition $\varphi = \varphi_0$ for $d_a = d_p$, which yields $a = 1$. This enables us to write

$$\varphi = 1 - (1 - \varphi_0)\left(\frac{d_p}{d_a}\right). \tag{4}$$

We can compute the porosity using Eq. (4) for the known d_a.

It is convenient to introduce the parameter characterizing the degree of friability of a packing:

$$D = (\varphi - \varphi_0)/(1 - \varphi_0) . \tag{5}$$

Equation (4) can be written in the form $D = 1 - d_p/d_a$.

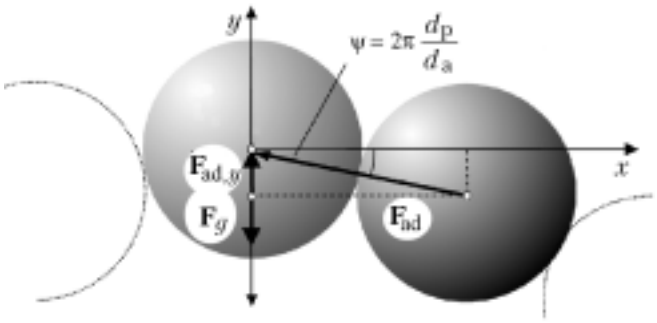

Fig. 4. Forces of interaction between particles in the agglomerate.

Stability of Agglomerates. The maximum size of an agglomerate in the sediment is determined by the ratio of the adhesive force of cohesion between particles and the force destroying the agglomerate. The gravity force acts as the cohesion force. The balance of the forces will be composed for a particle at the top of the agglomerate (this particle is the most sensitive to destruction (Fig. 4)).

The compressive stress σ_{at} between neighboring particles due to adhesion is $\sigma_{at} = F_{ad}d_p^{-2} = Ed_p^{-1}$, where E is interpreted within the DLVO theory as the adhesion energy [10]. The component of the compressive stress in the y direction is equal to

$$\sigma_y = \sigma_{at} \sin \alpha , \tag{6}$$

here $\alpha = 2\pi/m$ and

$$m = 2\pi \frac{d_a}{d_p} . \tag{7}$$

Using Eq. (7) for expression of the angle, we transform (6) into

$$\sigma_y = \frac{F_{ad}}{d_p^2} \sin \frac{d_p}{d_a} .$$

Each particle in the agglomerate's shell contacts more than one neighboring particle. The number of contacts is a random quantity varying between two and six. We can take "four" as the average value. The stress seeking to destroy the agglomerate formed is produced due to the gravity force F_g less the Archimedes force $\sigma_d = gL(\rho_p - \rho_1)(1 - \varphi)$. In this case the balance of stresses is as follows:

$$4 \frac{E}{d_p} \sin \frac{d_p}{d_a} = gL (\rho_p - \rho_{liq}) (1 - \varphi) . \tag{8}$$

When the d_p/d_a ratios are small, from Eq. (8) we find the agglomerate size

$$\frac{d_p}{d_a} = \frac{g\Delta\rho L (1 - \varphi) d_p}{4E} . \tag{9}$$

Having taken g = 10 m/sec^2, $L = 10^{-2}$ m, $d_p = 10^{-5}$ m, $\Delta\rho = \rho_p - \rho_{liq} = 10^{-3}$ kg/m^3, φ = 0.5, and $E = 5 \cdot 10^{-4}$ N/m for evaluations, we obtain $d_a = 4d_p$.

Porosity. Having substituted the value for $d_a >> d_p$ from Eq. (9) into Eq. (5), we obtain

$$\varphi = 1 - (1 - \varphi_0) \left(\frac{d_p}{d_a} \right) = 1 - (1 - \varphi_0) \frac{g\Delta\rho L (1 - \varphi) d_p}{4E} . \tag{10}$$

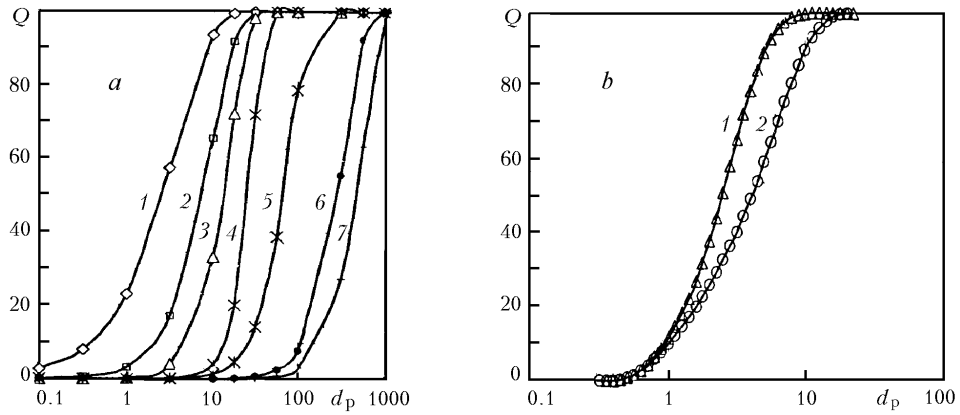

Fig. 5. Total size-distribution functions of glass (a) and sand (b) particles (measured by the optical method with a MasterSizerX device (Malvern Corp.)): a) 1) d_S = 3.7; 2) 9.6; 3) 15.7; 4) 29.2; 5) 80.4; 6) 370; 7) 560 μm; b) 1) SF-800; 2) SF-500.

It is easy to explicitly express the porosity from Eq. (10), but for simplicity of the final expression we take $\varphi = \varphi_0$ on the right-hand side and rewrite (10) in the form

$$\varphi = 1 - \frac{g\Delta\rho L\,(1-\varphi_0)^2\, d_p}{4E}\,. \tag{11}$$

The dimensionless parameter $g\Delta\rho L d_p/(4E)$ is the ratio of the gravity forces and the adhesion forces.

In accordance with formula (11), the porosity of the sediment layer must decrease in proportion to the layer thickness and the particle size. For a certain final thickness of the layer, the porosity, according to (11), vanishes, which, certainly, is a consequence of the adopted relation $d_a >> d_p$. To remove this "nonphysicality" we correct (11), considering this formula as the first term of the expansion of a certain appropriate expression with a plausible limit for $L \to \infty$ or for $d_p \to \infty$. For example,

$$\frac{\varphi - \varphi_0}{1-\varphi_0} \approx \frac{1}{1 + (1-\varphi_0)\, g\Delta\rho L d_p / 4E}\,. \tag{12}$$

Experiments. The aim of the experiments is to check the suitability of formulas (11) and (12) for evaluation of the sediment porosity. For this purpose we varied the particle size, the layer thicknesses, and the specific adhesive energy.

As the loose material we employed:

1. Glass spheres characterized by their average size in the form $d_S = 6V_p/S_p$, where V_p is the total volume of particles and S_p is the total surface area of particles, from 3.7 to 560 μm; the particle-size distribution is shown in Fig. 5a.

2. Fine-grained quartz sands SF-800 (d_S = 2.5 μm) and SF-500 (d_S = 4 μm); the particle distribution of these materials is shown in Fig. 5b. From the data of the producer (Frechen Corp.), quartz sands contain more than 99% SiO_2.

3. Kaolin (particles have the shape of plates). The average kaolin-particle size determined by the optical method was 4 μm.

We employed demineralized water as the liquid phase. In the corresponding cases we took the solution of an $MgCl_2$ or $AlCl_3$ electrolyte.

To produce a suspension of the quartz sands we prepared in advance solutions of $MgCl_2$ or $AlCl_3$ salts in demineralized water. The electrolytes of the inorganic salts acted as coagulating substances which accelerate the process of settling. The suspensions were dispersed with a laboratory mixer in five glass beakers for 45 min. To disperse a powder in the aqueous solution of salts one must select the optimum rate of mixing, characterized by the energy

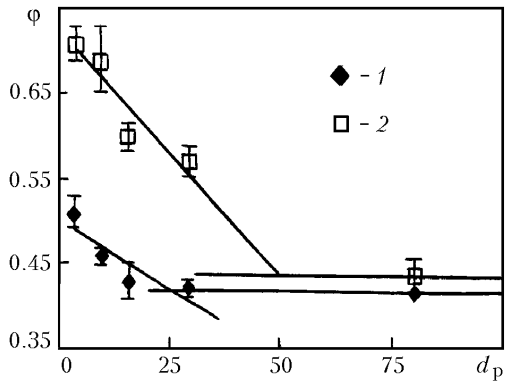

Fig. 6. Porosity as a function of the diameter of the glass particles: 1) sediment; 2) dry charge.

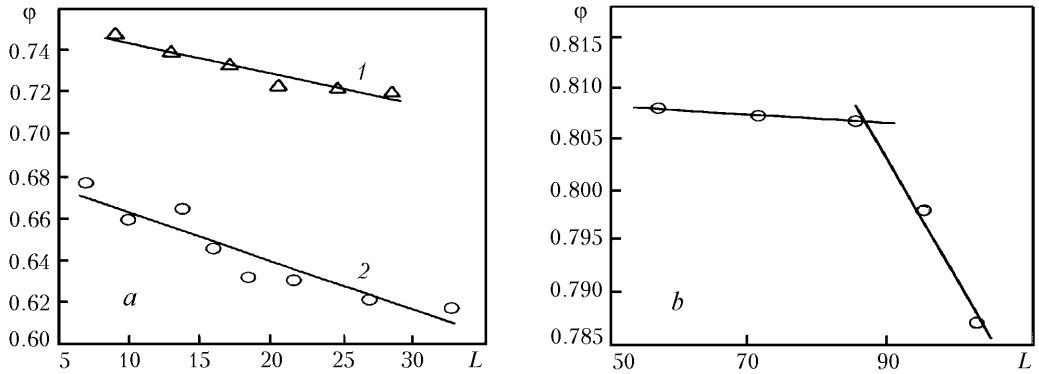

Fig. 7. Porosities of the sediment vs. its thickness: a) sand (1) SF-800, $y = 0.0014x + 0.757$; 2) SF-500, $y = 0.0023x + 0.685$); b) kaolin.

supplied. When the mixing rate is insufficiently high, particles are poorly entrained into the vessel and remain afloat. Taking these factors into account, we selected a propeller mixer ensuring sufficient energy supply for an angular rotational velocity of the mixer of 200 min^{-1}.

The concentration of the solid substance lay in the interval from 3 to 7% by volume.

The suspensions prepared were poured directly into measuring cylinders of height 35 cm and diameter 4.6 cm for their subsequent settling. The height of the sediments in the measuring cylinders was measured after the complete settling of the suspension, which lasted from 15 to 48 h depending on the particle size.

Results. Measurements of the porosity of a sediment in nondemineralized water (pH 7) as a function of the size of glass particles are shown in Fig. 6. Fairly pronounced are two regions: the linear dependence of the porosity on d_p is characteristic of small particles, approximately to 30 μm in diameter, whereas practically the total independence of the porosity from the size is characteristic of large (> 30 μm) particles. As the particle size increases, the porosity tends to a value of 0.41, which lies in the interval usually indicated for φ_0. For the sake of comparison, Fig. 6 gives the dependence of the porosity on the sphere size in an ordinary sedimentation experiment and the similar dependence for a dry charge. The latter was obtained through charging slowly a certain mass of glass spheres into a measuring cylinder. Again, the porosity was determined from the height of the charge layer formed.

It is seen that the porosity of the dry charge is much higher than that of the sediment, although the qualitative dependences on the particle size are identical in both layers. The reason for the higher-than-average porosity in the case of the dry charge is capillary forces acting in addition to van der Waals forces. The natural content of water measured thermogravimetrically on particles of different diameter ranged between 0.06 and 0.1%, which would correspond to a liquid film of thickness 10 nm or higher. The dependence $\varphi(d_p)$ (Fig. 6) can completely be described by formula (12).

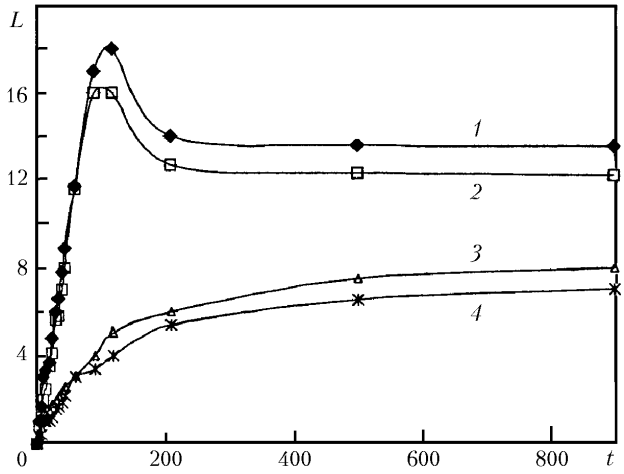

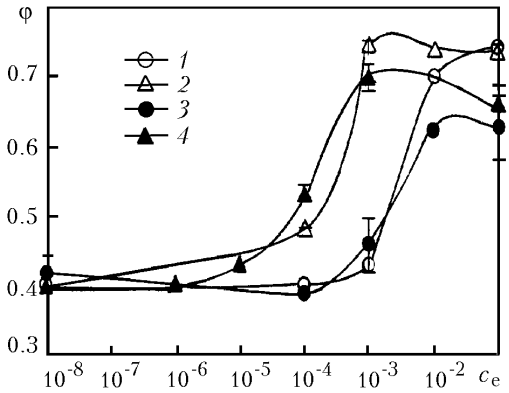

Fig. 8. Dynamics of growth of the sand-sediment layer (material SF-500) for different concentrations of $MgCl_2$ (mole/liter): 1) 10^{-1}; 2) 10^{-2}; 3) 10^{-3}; 4) 10^{-4} (demineralized water).

Fig. 9. Porosities of the settled layer of sand vs. concentration of the electrolytes: 1) $MgCl_2$, SF-800; 2) $AlCl_3$, SF-800; 3) $MgCl_2$, SF-500; 4) $AlCl_3$, SF-500.

Figure 7a represents a check of theoretical conclusions for the dependence of the porosity on the layer thickness. In this case, we have employed fine-grained particles of quartz sand. A situation similar to that described above is observed: for thin sediment layers the porosity is in proportion to the thickness of a sediment layer, whereas for relatively thick layers the porosity depends on the thickness only slightly.

In the region of thin sediments, $d\varphi/dL$ must be in proportion to the diameter of the particle material. Comparing the slopes of the curves for SF-500 sand ($d_S \approx 4$ μm) and for SF-800 sand ($d_S \approx 2.5$ μm), we can see that this statement holds quite well — the slopes correlate with each other approximately as 1.64 whereas the particle sizes correlate as 1.6. Unlike formula (11), for $L \to 0$ the experimental curves, even if they seek to converge to a single point, converge to a value of $\varphi \approx 0.7$ rather than $\varphi = 1$. Naturally, for $L \to 0$ the notion of a layer and the applicability of formula (11) lose their meaning. Finally, one more circumstance is worth noting. For higher L we have recorded the practical independence of φ from L, but, unlike formula (12), the limiting value of φ is still very far from $\varphi \approx 0.4$.

Figure 7b demonstrates, in our opinion, the influence of the particle shape. Kaolin particles represent plates which, superimposing on one another, form a strong packing, as we can imagine. Therefore, in the case of thin layers the structure formed in the course of sedimentation successfully resists the pressure of the particles lying above and these structures are transformed only for a sufficient thickness of the sediment, which leads to a linear drop in the porosity as a function of the layer thickness.

It is more difficult to show the influence of E on the sediment porosity, since direct measurements of this quantity are few in number. In what follows, we will employ data [13] obtained by the centrifugal method for an SiO_2–H_2O–SiO_2 system in an aqueous solution of $MgCl_2$. Figure 8 shows the dynamics of growth of a sediment layer for different concentrations of $MgCl_2$. We can differentiate two regimes of formation of the layer. When the concentrations of the electrolyte are low, the layer increases monotonically, but when the concentrations are fairly high, the layer thickness varies nonmonotonically with time and the establishment of the final state is accompanied by shrinkage of the layer. For low concentrations of the electrolyte we have a simple layer-by-layer precipitation of individual particles forming a relatively dense packing with $\varphi = \varphi_0$. If the concentration of the electrolyte is fairly high, particles precipitating from the solution onto the sediment surface form complex structures with a very friable packing by virtue of their strong tendency to adhesion, which has schematically been described in the model presented above. The newly formed layers apply pressure to those lying below, and if the stability limit of the aggregates in the latter is exceeded, the aggregates, changing to smaller ones, are destroyed — the compaction of the sediment occurs. The final state is described by the model presented.

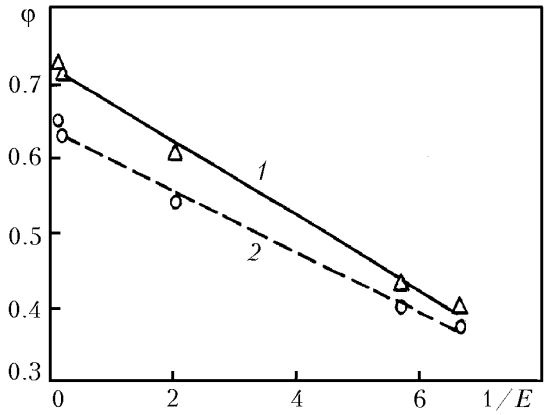

Fig. 10. Correlation between the porosity and the adhesive energy: 1) SF-800; 2) SF-500.

Recording the values of porosity for a completely established layer (approximately after 15–48 h) for different concentrations of the electrolyte, we can see that the sensitivity of the porosity to the concentration of $MgCl_2$ is strong only in a fairly narrow interval of variation of the electrolyte concentration (Fig. 9). The adhesive energy sharply changes in the same interval (see Fig. 7).

Figure 9 also shows a change in the porosity of the settled layer for two materials of different grain size and for two different electrolytes — $MgCl_2$ and $AlCl_3$. The sediment of the finer material possesses a higher porosity, particularly in the region of a high concentration of the electrolytes, which follows from the model.

The interval of concentrations of a rapid porosity growth for the trivalent electrolyte lies in the region of lower values than that for the bivalent electrolyte, which is consistent with the Schultz–Hardy rule reflected by formula (2). True enough, quantitative agreement between the measurements and this rule is available only for the fine-grained sand SF-800; for the larger-grained SF-500 the agreement is only qualitative.

Let us draw on the fact that the measured forces (energies) of adhesion for the SiO_2 system in the solution of $MgCl_2$ are known [13]. The correlation between the porosity and the adhesive energy for the case of this solution is shown for two materials — SF-500 ($d_S \approx 4.0$ μm) and SF-800 ($d_S \approx 2.5$ μm) — in Fig. 10. Although the correlation is nearly linear, it should be noted that the slopes of regression curves for these two variants differ by only 20% instead of the expected 60% predicted by theory.

NOTATION

A, Hamaker constant, J; a, dimensionless parameter; c_∞, concentration of ions in the liquid at a large distance from the particle surface, m^{-3}; c_{cr}, concentration of the electrolyte, critical for coagulation, mole/liter; c_e, concentration of the electrolyte, mole/liter; D, parameter characterizing the degree of friability of the packing; d_a, agglomerate diameter, m; d_p, particle diameter, m; d_m, molecular size, m; d_S, average diameter of particles, m; e, elementary charge, C; E, specific surface energy of adhesion, N/m; F_{ad}, adhesion force, N; F_{at}, attracting component of the adhesive force, N; F_B, Born force, N; F_g, gravity force, N; F_r, repelling component of the adhesive force, N; g, free-fall acceleration, m/sec^2; h, distance between the surface of interacting particles, m; k, Boltzmann constant, J/K; L, sediment thickness, m; m, number of particles along the perimeter of the agglomerate; n, number of particles in the agglomerate; S_p, total area of the particle surface, m^2; t, time, sec; T, temperature, K; V, elementary volume, m^3; V_a, volume occupied by the agglomerate, m^3; V_p, total volume of particles in the layer, m^3; W, force potential, V; W_{at}, attractive potential, V; W_r, repulsive potential, V; z, valence of an ion; α, effective angle of opening in the agglomerate, rad; β, constant; ε and ε_0, dielectric constants, $C^2/J/m$; φ, porosity of the layer; φ_0, porosity of the random packing; ψ_0, potential of the particle surface, V; $1/\kappa$, Debye length, m; ρ_p, density of the particle material, kg/m^3; ρ_{liq}, density of the liquid, kg/m^3; $\Delta\rho$, difference of the densities of the particle material and the liquid, kg/m^3; γ, dimensionless parameter; σ_{at}, compressive stress, N/m^2; σ_d, stress seeking to destroy the agglomerate, N; σ_y, component of the compressive stress,

N/m^2. Subscripts: a, agglomerate; ad, adhesion; at, attraction; B, Born force; cr, critical; d, destructive; e, electrolyte; liq, liquid; p, particle; m, molecule; r, repulsion; S, average (according to Sauter); *y*, direction along the *y* axis.

REFERENCES

1. W. H. McAnally and A. J. Mehta, *Coastal and Estuarine Fine Sediment Processes*, Elsevier, Amsterdam–London–New York–Oxford–Paris–Shannon–Tokyo (2001).
2. A. Rushton, A. S. Ward, and R. G. Holdich, *Solid-Liquid Filtration and Separation Technology*, VCH, Weinheim–New York–Basel–Cambridge–Tokyo (1996).
3. R. J. Wakemen, M. N. Sabri, and E. S. Tarleton, Factors Affecting the Formation and Properties of Wet Compacts, *Powder Technol.*, **65**, 283–292 (1991).
4. E. Zvetanov, J. Dueck, and Th. Neeβe, Untersuchungen zur Porosität feinkörniger Filterkuchen, *Chem. Ing. Techn.*, **71**, No. 8, 835–839 (1999).
5. C. Kranenburg, The Fractal Structure of Cohesive Sediment Aggregates, *Estuarine, Coastal and Shelf Sci.*, **39**, 451–460 (1994).
6. K. Taki, Critical shear stress for cohesive sediment transport, in: W. H. McAnally and A. J. Mehta (Eds.), *Coastal and Estuarine Fine Sediment Processes*, Elsevier, Amsterdam–London–New York–Oxford–Paris–Shannon–Tokyo (2001).
7. J. Dueck, E. Zvetanov, and Th. Neeβe, Porositätsmodell für feinkörnige Filterkuchen, *Chem. Ing. Techn.*, **71**, No. 7, 692–696 (1999).
8. J. Dueck, E. Zvetanov, D. Purevjav, and Th. Neesse, Influence of Surface Forces on the Porosity of the Fine-Grained Filter Cakes, in: *Proc. 14th Int. Congr. of Chemical and Process Engineering CHISA 2000*, Praha, Czech Republic, Summaries, Vol. 2, Separation Process and Equipment. August 2000, p. 175.
9. J. Israelachvili, *Intermolecular & Surface Forces*, Academic Press, San Diego (1995).
10. H. Krupp, Particle Adhesion — Theory and Experiment, *Adv. Colloid Interface Sci.*, **1**, 111–239 (1967).
11. Van Oss and J. Carel, *Interfacial Forces in Aqueous Media*, Marcel Dekker, New York (1994).
12. R. Hein, Th. Hucke, M. Stinz, and S. Ripperger, Analysis of Adhesion Forces between Particles and Wall Based on the Vibration Method, *Particle & Particle System Characterization*, **19**, 269–276 (2002).
13. K. Muehle, K. Domasch, and Th. Neeβe, Zur physikalisch begründeten Modellierung des Flockungsprozesses, *Chem. Tech.*, **34**, 14–18 (1982).
14. A. D. Zimon and R. F. Leshcenko, *Colloidal Chemistry* [in Russian], Agar, Moscow (2001).
15. K. S. Krasnov (Ed.), *Physical Chemistry* [in Russian], Vysshaya Shkola, Moscow (2001).